Robotica (2016) volume 34, pp. 1553–1565. © Cambridge University Press 2014
doi:10.1017/S0263574714002446

A caterpillar climbing robot with spine claws and compliant structural modules

Wei Wang and Shilin Wu*

Robotics Institute, School of Mechanical Engineering and Automation, Beihang University, Beijing, P. R. China

(Accepted September 9, 2014. First published online: October 15, 2014)

SUMMARY

This paper proposes a modular caterpillar climbing robot using spines as the attaching tools. To improve the reliability of the spines' engagement and disengagement, this paper discusses the reasonable trajectory of the spine and designs a driving mechanism of the spine based on the compliant mechanism theory. Then some compliant modules are designed and realized to build the caterpillar climbing robot. A climbing gait is designed to avoid collisions between the spines and the wall, and allows the robot to climb on a stucco-like wall with a 72° incline. The real tests reveal that the deformation of the compliant toes reduces the sliding forces between the spines and the wall, and improve the climbing action obviously.

KEYWORDS: Caterpillar robot; Climbing robot; Bionic robot; Compliant module; Spine claws.

1. Introduction

Wall climbing robots may complete a variety of tasks, such as post-disaster rescue, engineering test, etc. Currently, most climbing robots use the following traditional attaching methods: magnetic adsorption,[1,2] cups or vacuum adsorption,[3,4] and electrostatic adsorption.[5] However, those traditional methods are limited by some disadvantages: (i) consuming high energy (even when a robot is stationary) on magnetic and electrostatic adsorption, (ii) involving complex auxiliary devices to generate the attach force, and (iii) only suitable for attaching to smooth, clean, and even surfaces. Methods inspired by animals in nature, such as crawls,[6] spines,[7] and "dry adhesion" using van der Waals forces for attachment,[8–10] are researched to overcome those disadvantages. Ref. [6] introduced a robot which mimicked the kinematics of a human rock climber to climb on vertical surfaces by virtue of claws and had the ability to stay statically hanging on the wall with no energy consumption. Ref. [11] described another biomimetic approach which used an array of micro spines to scale vertical walls such as brick, concrete, stucco or stone. With a compliant attachment mechanism, Spinybot-II ensured a good mechanical contact, as well as low power consumption, lightweight and being independent of material contaminants or dust on a surface.

Besides the passive attachment tools as spines, the compliant mechanism and flexible or elastic components are applied more and more frequently in climbing robots. The reason is that the compliant mechanism can simplify the manufacture and assembly and reduce the weight, which is a key point in the climbing robot design. Flexible or elastic components can change the structure stiffness, storage the energy during robot moving, thus the contacting forces between robots and environment can be reduced. Ref. [12] described a biomimetic robot inspired by inchworm which could travel along rough surfaces, leaf edges, and boughs of tree. To generate a turning motion, flexible polymer films and composites were used to constitute flexure joints. Ref. [13] described a hybrid aerial and scansorial robotics which could land and attach to vertical wall using spines. Those spines engaged and disengaged on the asperities with high adaptability by utilizing a compliant driving mechanism. Ref. [14] introduced a flexible tree climbing robot which could reach many places of a tree, by virtue of a compliant gripper holding mechanism. JPL (American Jet Propulsion Laboratory) developed

* Corresponding author. E-mail: wsl.54@163.com

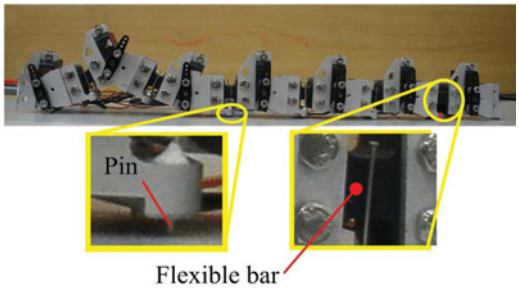

Fig. 1. Seven-joint climbing caterpillar robot in ref. [16].

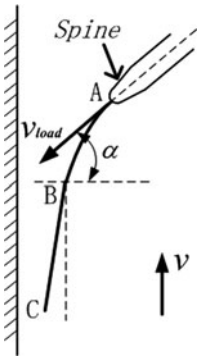

Fig. 2. Ideal trajectory of a spine.

the first rock climbing robot with grippers that each could support 750 N in any direction. This multi-legged robot was of excellent ability to climb cater walls, and cliff faces.[15]

To expand the climbing ability of the caterpillar climbing robot to non-flat surfaces, the authors of this paper combines the spine-based compliant attachment mechanism with the modular caterpillar climbing robot concept. Our previous work built a caterpillar robot using flexible natural rubber bars as connecting components,[16] as shown in Fig. 1. A series of experiments revealed that the side-sliding forces and energy consumption were reduced by the flexible components. The findings encourage us to design a new caterpillar robot based on the compliant mechanism.

This paper is organized as follows: in Section 2, we firstly discuss the spine trajectory which is suitable for the caterpillar climbing robot to engage asperities and a compliant mechanism driving the spines. Then, we build a model of one robot module for calculating and evaluate its stiffness which influences the performance of the spine engagement. The simulation of engagement by the ADAMS software is also presented and the spine trajectory is plotted by MATLAB which testify our analyses. In Section 3, the modules are designed and a prototype is assembled. Then, the climbing gait of the new designed caterpillar robot is presented and analyzed in Section 4. To test and verify the feasibility of the above theories and analyses, experiments are performed on stucco-like wall in Section 5. Finally, some conclusions and future work are outlined.

2. The Engagement Trajectory and Flexible Mechanism Design of the Spine

2.1. The engagement trajectory of the spine

To reliably engage on the wall, a spine should move towards the wall on an ideal trajectory which comprises two curves,[17] as shown in Fig. 2. The first one is the curve AB. In this stage, the spine is not in contact with the surface and brought downward to the wall. v_{load} is the velocity vector of the spine tip. The approach angle α, which is measured between the direction of the vector v_{load} and the direction normal to the climbing surface, is vital for the spine to perch on an asperity of the wall.

An undesirable α may lead the spine finding no asperities to catch on. According to ref. [17], α should be approximately between 45° and 65°. The second curve is an approximate straight line BC which is in the direction of being down along the wall. It presents a movement that the spine is being

https://doi.org/10.1017/S0263574714002446 Published online by Cambridge University Press

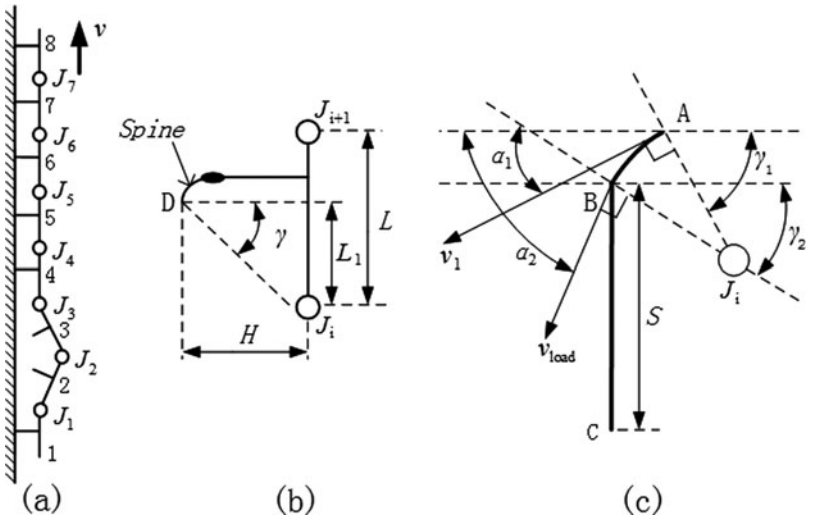

Fig. 3. Ideal trajectory of a spine.

dragged down along the wall by a driving mechanism when it touches the wall. Considering the specific structure of the caterpillar robot, the detached trajectory can be treated as the reverse process of attachment.

The actual trajectory of a spine is determined by the mechanical configuration of the caterpillar robot.[18] In Fig. 3, one module of the caterpillar robot is simplified to a link with one spine. Fig. 3 (a) shows a caterpillar robot model which is composed of eight identical modules and seven active rotating joints to connect the modules to a chain like configuration. The dimension of single module is also presented in Fig. 3 (b). The point D stands for the tip of a spine, L is the distance between two adjacent joints, H is the distance from point D to line J_iJ_{i+1}, L_1 is the distance from the projection of point D on line J_iJ_{i+1} to point J_i. The ideal trajectory of the spine's tip is shown in Fig. 3 (c). The first curve is a circular arc due to the rotation of the joint. α_1 is the initial approach angle and α_2 is the ending approach angle. According to ref. [17], α_1 and α_2 should satisfy the inequality (1):

$$45^\circ \leq \alpha_1 \leq \alpha_2 \leq 65^\circ. \tag{1}$$

Since $\gamma 1 = 90^\circ - \alpha 1$ and $\gamma 2 = 90^\circ - \alpha 2$.
Then γ can be deduced:

$$25^\circ \leq \gamma_1 \leq \gamma \leq \gamma_2 \leq 45^\circ. \tag{2}$$

According to Fig. 3 (b), the relationship between γ and L1, H is:

$$\tan\gamma = \frac{L_1}{H}. \tag{3}$$

Three rules must be followed when the engaging action is in the second part of the trajectory.

1. The projection of the spine tip's instant velocity on vertical direction must be opposite to the climbing direction.
2. The spine tip should keep contacted with the wall in process of being dragged down along the wall.
3. The spine must be driven passively to reduce the sliding force acting on the attached spines of other modules.

A diving mechanism connecting the spine to the module is designed to fulfill the above rules. Fig. 4 (a) shows the compliant four-link mechanism. The first rule can be followed by trajectory planning of the spine tip E on the coupler of a planar four-link mechanism, as shown in Fig. 4 (b). If the instant velocity center O of link CD is on the right of point E (the spine tip) fixed to link CD and AC+CD>AB+BD, the first rule can be followed. When link AB contacts with the wall, it is

https://doi.org/10.1017/S0263574714002446 Published online by Cambridge University Press

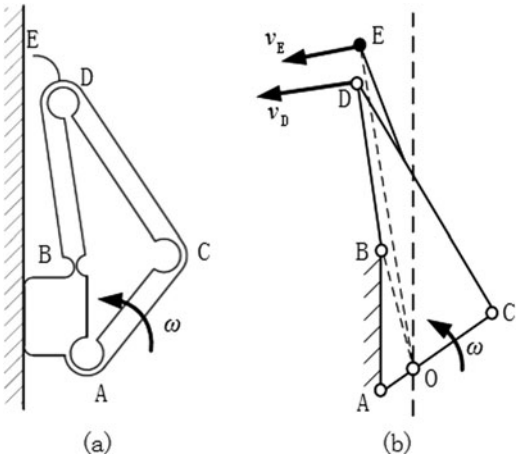

Fig. 4. The compliant diving mechanism of spines.

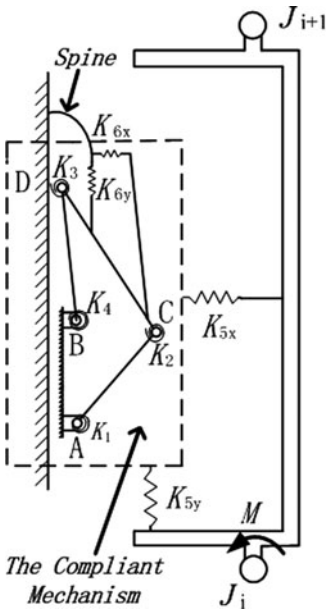

Fig. 5. The model of one module.

assumed stationary or can only move along the wall during the robot climbing. Link AC is fixed to the robot module. A spine is fixed to link CD. Joint A is driven by a servo motor.

2.2. The mechanical model of one module based on compliant spine mechanism

To reduce the sliding and collision forces between the spine and the asperity, the spine is connected to the module frame via a flexible allocation or compliant hinges as shown in Fig. 5.

Assuming that K_x is the stiffness of a spine in the horizontal direction and K_y is the stiffness in the vertical direction. K_x should be large so that the spine can disengage effectively and a larger K_x can also prevent spines from occasionally jamming in deep pits during disengagement. K_y should be small to increase the probability for a spine to catch an asperity during being dragged down along the wall.

As we know, the stiffness of a four-link compliant mechanism is too large in both the vertical and the horizontal directions for a spine to engage or disengage an asperity. To deduce the stiffness, two linear springs or flexible components are connected in series to the compliant mechanism, which effectively amplifies the displacement of a spine.

https://doi.org/10.1017/S0263574714002446 Published online by Cambridge University Press

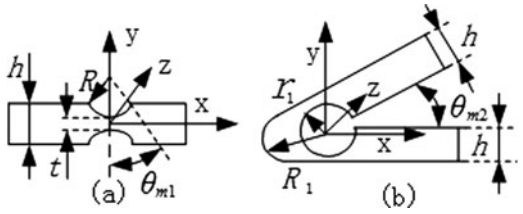

Fig. 6. Two types of flexure hinges.

Combining the above analyses together, a mechanical model of one module is built without considering the damping. J_{i} and $J_{\mathrm{i+1}}$ are joints that connect successively with one module. K_1, K_2, K_3, K_4, are the stiffness of the twisted springs at joint A, B, C, D, when the compliant mechanism is simplified according to the pseudo-rigid-body model theory. $K_{5\mathrm{x}}$ and $K_{5\mathrm{y}}$ are the stiffness of the components connecting the compliant mechanism to one module, and should be large enough to decrease their effects on spines' movement. $K_{6\mathrm{x}}$ and $K_{6\mathrm{y}}$ are the stiffness of the linear springs or flexible components connecting the spines.

2.3. Estimation of K_1, K_2, K_3, K_4

There are two types of flexure hinges used in the design of a planar four-link compliant mechanism.[17] One is the right circular flexure hinge in Fig. 6 (a) and another is the acute angle flexure hinge in Fig. 6 (b). The rotational stiffness K around Z-axis can be calculated by Eq. (4) and is constant in circumstance of small deformation. E is the Young's modulus, b is the length along Z-axis, h is the length along Y axis, t is the smallest thickness along Y axis of the left hinge, R is the radius of the arc circular of the left hinge, θ_{m1} is half of the arc circle angle of the left hinge.

$$K = EbR^2/12f_1 \tag{4}$$

For the first type flexure hinge shown in Fig. 6 (a), f_1 can be approximated by Eq. (5), while the stiffness of the second hinge type shown in Fig. 6 (b), can be predicted by Eq. (7)

$$f_1 = \frac{8r^4(2r+1)\tan\frac{\theta_m}{2}}{(4r+1)^2\left[1+(4r+1)\tan^2\frac{\theta_m}{2}\right]^2} + \frac{8r^3\left(6r^3+3r+1\right)\tan\frac{\theta_m}{2}}{(4r+1)^2\left[1+(4r+1)\tan^2\frac{\theta_m}{2}\right]} + \frac{12r^4(2r+1)}{(4r+1)^{5/2}}\arctan\left(\sqrt{4r+1}\tan\frac{\theta_m}{2}\right), \tag{5}$$

where r can be attained by Eq. (3):

$$r = R/t \tag{6}$$

$$f_1 = \int_{-\frac{\theta_m}{2}}^{\frac{\theta_m}{2}} \frac{\cos\theta}{\left(\frac{R_1-r_1}{R_1}+1+\cos\theta\right)^3} d\theta, \tag{7}$$

where r_1 is the radius of the internal circle and R_1 is the radius of the externally tangent circle. θ_{m2} is the angle of the two tangent lines of the R_1 circle.

2.4. Estimation of joint driving torque based on the mechanical model of the spine

Figure 7 shows a typical moment when the climbing caterpillar robot is moving upward with only four middle joints 2, 3, 4, and 5 turning, and the spine of module 3 is just contacting with the wall. The other modules have already attached on the wall. The forces acting on the robot are also shown in Fig. 7. $F_{\mathrm{xi}}(i = 1, 2, 3, 6, 7, 8)$ and F_{yi} are forces from the asperities to the spines. The distance from point A to point B is k^*L. m is the mass of one module, g is the gravity acceleration.

https://doi.org/10.1017/S0263574714002446 Published online by Cambridge University Press

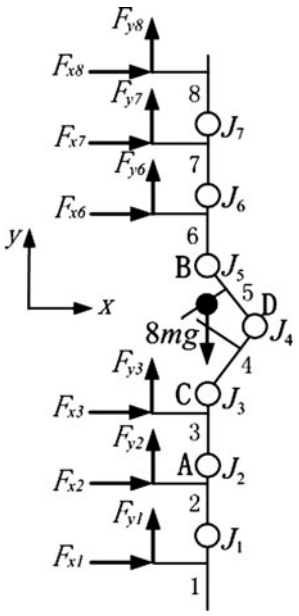

Fig. 7. Forces acting on the robot.

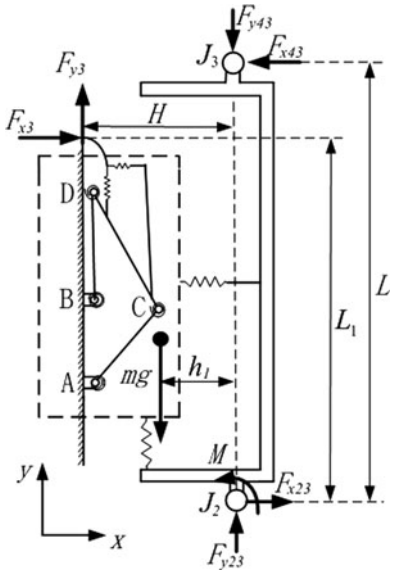

Fig. 8. Static model of the module 3.

Figure 8 shows the static model of module 3. The driving torque M for the joint of the module 3 can be obtained by Eq. (8).

$$M = 4mg \cdot \left(\frac{2HL_1 - 6k_1LH}{3kk_1L + 8k_1L - 2L} + \frac{2H}{5k_1 + 1} - \frac{h_1}{4} \right). \tag{8}$$

2.5. Estimation of K_{6x} and K_{6y}

To enable the spines to engage more reliably, the displacement Δy of the spring or the flexible component is far larger than the displacement Δx, as shown in Fig. 9. Given the Δy and Δx, K6x and K6y can be estimated by the equilibrium condition of forces at the spine.

$$K_{6x} = F_{x3}/(N\Delta x) \quad K_{6y} = F_{y3}/(N\Delta y). \tag{9}$$

https://doi.org/10.1017/S0263574714002446 Published online by Cambridge University Press

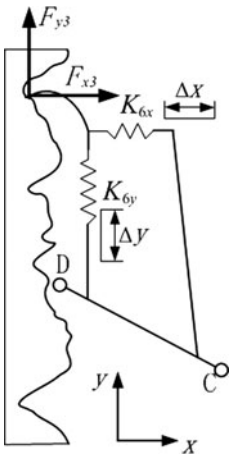

Fig. 9. Static model of a spine.

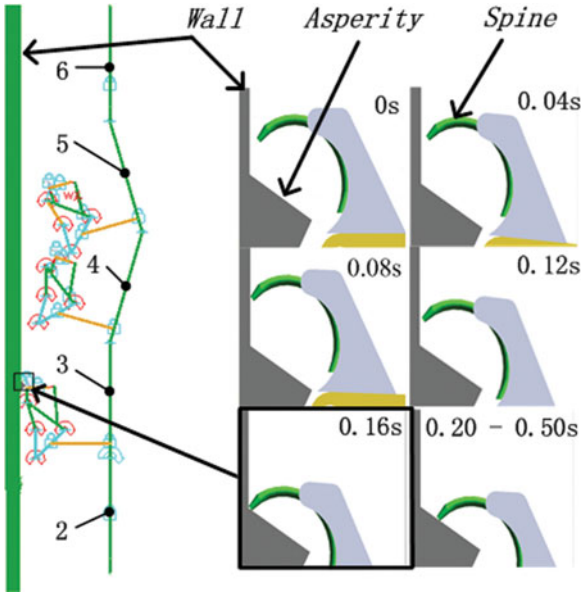

Fig. 10. The process of engagement of a spine.

where, N is the number of parallel compliant driving mechanisms of one module. According to Eq. (9), the two springs or flexible components can be chosen.

2.6. Simulations and results

To testify our analysis and the feasibility of the diving mechanism for attachment, a simplified model for one module is built with kinematical constraints in ADAMS/view. The material chosen for the four-link compliant mechanism is Polypropylene. The design parameters are as follows: $E = 2e9$Pa, $L = 20$ mm, $L_1 = 17$ mm, $H = 30$ mm, $b = 2$ mm, $R = 3$ mm, $t = 1$ mm, $R_1 = 3$ mm, $r_1 = 2$ mm, $\theta_{m_1} = 92°$, $\theta_{m_2} = 60°$, $30\,°$, $86\,°$. By Eqs. (4)–(7), $K_1 \approx 2.6$N*mm/deg, $K_2 \approx 2.3$N*mm/deg, $K_3 \approx 4.1$N*mm/deg, $K_4 \approx 1.3$N*mm/deg, $K_{6x} = 0.85$N/mm, $K_{6y} = 0.12$N/mm.

Figure 10 shows the simulation process when module 2 and 6 are fixed on the vertical wall. Firstly the link AB (in Fig. 4) of module 3 contacts with the wall, with an approach angle α of $50°$. Then the spine is dragged down along the wall due to the deformation of the planar four-link compliant mechanism when joint 2 keep pushing module 3 to the wall. Finally the spine engages on an asperity, with a clockwise torque imposed on the module 3. The simulation time is 0.5 s.

The displacement data of the spine tip are exported to MATLAB for plotting the trajectory, as illustrated in Fig. 11. The curve AB is an approximate circular arc and the line BC is an approximate

https://doi.org/10.1017/S0263574714002446 Published online by Cambridge University Press

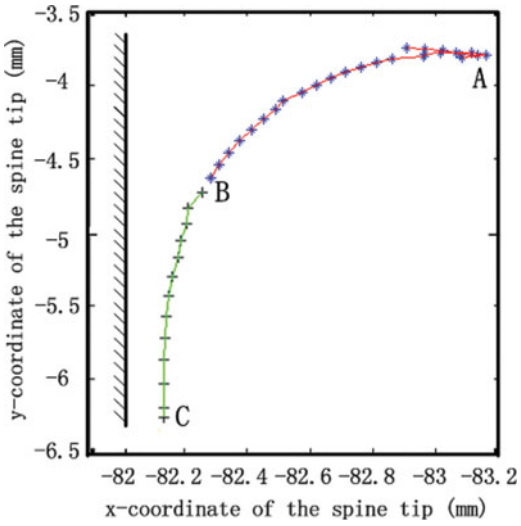

Fig. 11. The spine trajectory attained by simulation.

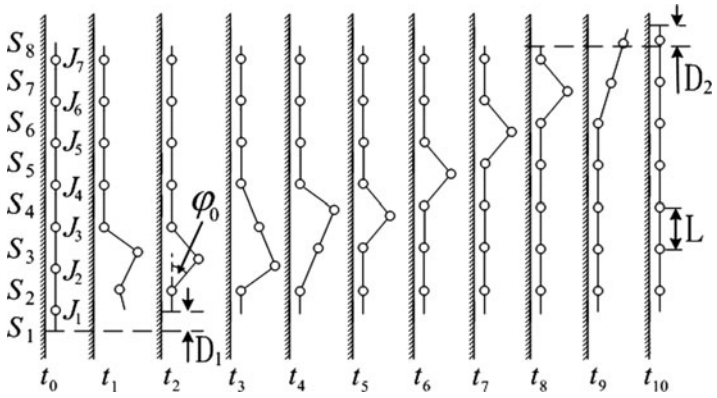

Fig. 12. One moving cycle (t_0–t_{10}) of the caterpillar robot's climbing gait is divided into three stages: two open-chain states (t_0–t_2 and t_8–t_{10}) and one closed-chain (t_2–t_8) state. L is the length of one arthromere. The initial step length (D_1) and angle (φ_0) in the closed-chain is transmitted from arthromere S_1 to S_8. D_2 is the eventual step length, and also the robot's actual step length after one moving cycle.

straight line leaning down towards the wall, which fulfills the desired trajectory proposed before. The compliant mechanism is proven to be valid for driving the spine.

3. Climbing Gait Analysis of the Robot

Inspired by the bionics research results, one moving cycle of a caterpillar robot consists of three states, when one body wave propagates from the tail arthromere to the head arthromere.

The robot's gait is shown in Fig. 12, the processes $t_0 \sim t_1$ and $t_9 \sim t_{10}$ are called open-chain states while the process $t_1 \sim t_9$ is called closed-chain state. The deformation of the arthromeres and spines is omitted so as to simplify the analysis. In the closed-chain state, the moving joints and linkages can be treated as a four-link mechanism, which has one DOF and four driving joints. To avoid conflicts among these joints, only one joint is appointed as the active joint, and other three joints follow it to rotate. In this paper, we called these joints 'passive joints'. In addition, due to the foot sliding and body deformation caused by the structure and control deviations, the eventually step length D_2 is normally unequal to the initial step length D_1. However, to simplify the theoretical model, the deviation is neglected in our analysis.

To deduce the kinematic relation between the active joint and the passive joints, the process of the closed-chain state is chosen to be analyzed for a gait control programming. During the close-chain state (process t_2 to t_8 in Fig. 12), the wall-climbing gait can be described as procedure which a body

https://doi.org/10.1017/S0263574714002446 Published online by Cambridge University Press

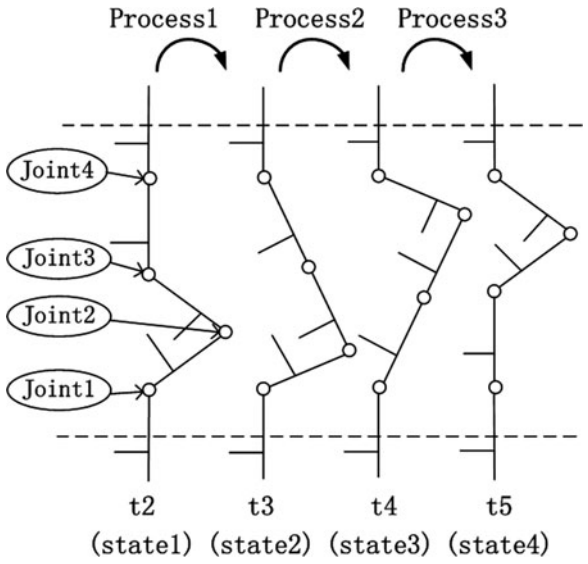

Fig. 13. One pulse in the closed-chain gait which convert state1 to state 4. Other two transitional states (state 2 and state 3) are inserted in to facilitate theoretical analysis.

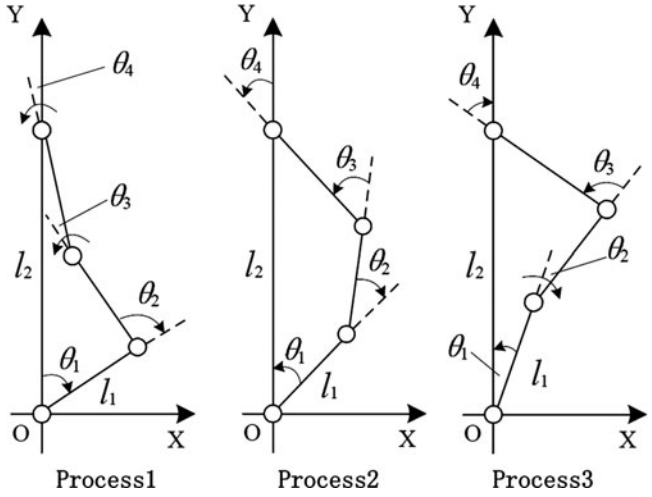

Fig. 14. The theoretical model during one pulse, which we simplify a partial caterpillar robot to a four-link mechanism according to the robot's dimensions.

wave is continuously transferred from one arthromere to an adjacent one, and then, repeated up to the top. Furthermore, the process (t_2 to t_5 in Fig. 12) can be considered as a typical pulse that will be used to describe one step. To calculate the moving joint angles during robot climbing, one pulse can be simplified as the movement of four-link mechanism instantaneously.

As shown in Fig. 13, one pulse is divided into three procedures, from process 1 to process 3. 'State 1' and 'State 4' can be regarded as the beginning and end states of one pulse via 'State 2', and 'State 3'. When a pulse passes away, joint 1 will change from the active state into the leisure state until the next pulse arrives.

The kinematical model of one pulse is illustrated in Fig. 14. The values of the joints' angle in one pulse can be calculated according to Eqs. (10)–(13) based on our previous work ref. [19].

$$\begin{cases} \theta_1(t) = \varphi_0 + \frac{\theta_{\max} - \varphi_0}{t_3 - t_2} \cdot (t - t_2) \\ \theta_2(t) = -\theta_1(t) - \arccos \frac{\delta(t)}{2} - \arcsin \frac{\sin \theta_1(t)}{\delta(t)} \\ \theta_3(t) = 2 \arccos \frac{\delta(t)}{2} \\ \theta_4(t) = \arcsin \frac{\sin \theta_1(t)}{\delta(t)} - \arccos \frac{\delta(t)}{2} \\ t \in [t_2, t_3) \end{cases} . \tag{10}$$

https://doi.org/10.1017/S0263574714002446 Published online by Cambridge University Press

$$\begin{cases} \theta_1(t) = \varphi_{\max} + \frac{\theta_{\mathrm{mid}} - \varphi_{\max}}{t_4 - t_3} \cdot (t - t_3) \\ \theta_2(t) = -\theta_1(t) + \arccos\frac{\delta(t)}{2} - \arcsin\frac{\sin\theta_1(t)}{\delta(t)} \\ \theta_3(t) = -2\arccos\frac{\delta(t)}{2} \\ \theta_4(t) = \arccos\frac{\delta(t)}{2} + \arcsin\frac{\sin\theta_1(t)}{\delta(t)} \\ t \in [t_3, t_4) \end{cases} . \tag{11}$$

$$\begin{cases} \theta_1(t) = \varphi_{\mathrm{mid}} - \frac{\theta_{\mathrm{mid}}}{t_5 - t_4} \cdot (t - t_4) \\ \theta_2(t) = -\theta_1(t) + \arccos\frac{\delta(t)}{2} - \arcsin\frac{\sin\theta_1(t)}{\delta(t)} \\ \theta_3(t) = -2\arccos\frac{\delta(t)}{2} \\ \theta_4(t) = \arccos\frac{\delta(t)}{2} + \arcsin\frac{\sin\theta_1(t)}{\delta(t)} \\ t \in [t_4, t_5) \end{cases} . \tag{12}$$

where

$$\begin{cases} \theta_{\max} = \arccos\frac{2\cos^2\varphi_0 + 2\cos\varphi_0 - 1}{1 + 2\cos\varphi_0} \\ \theta_{\mathrm{mid}} = \arccos\frac{\cos^2\varphi_0 + \cos\varphi_0 + 1}{1 + 2\cos\varphi_0} \\ \delta(t) = \sqrt{(1 + 2\cos\varphi_0)^2 - 2(1 + 2\cos\varphi_0)\cos\theta_1(t) + 1} \\ \theta_{\max} \in \left(0, \frac{\pi}{2}\right) \\ \theta_{\mathrm{mid}} \in \left(0, \frac{\pi}{2}\right) \end{cases} . \tag{13}$$

The solution is given by MATLAB and three processes from t_2 to t_5 are distinguished by colors, as shown in Fig. 15 (A). $\theta_1 - \theta_4$ are the angle values of joint 1 to joint 4 (see Fig. 13), and $t_2 - t_5$ of the time-axis represent one cycle of the pulse transmission. Since the change of angle value is not smooth in the initial result, the three order approximations are used to alternate the original data in the perspective of controller development, as shown in Fig. 15(B).

4. The Prototype and Experiments

One compliant module corresponding to one body arthromere is shown in Fig. 16 (the body module). The head and the tail modules are part of the body module. For reliable attachment on a rough surface, one module contains an array of five individual-compliant micro spines as its toes, see Fig. 17. Each toe is capable of carrying a small fraction of the total weight independently due to the deformation. When many toes make stable contact with asperities on a surface, force in the fore-after direction is distributed throughout a module. Furthermore, the total weight of the robot will be distributed among modules if majority of the micro spines contact with the wall.

Considering its excellent performance of light weight and high strength, nylon is chosen to build the modules by virtue of the laser sintering rapid prototyping technology. The assembled caterpillar robot consists of eight modules including the head and the tail. One FUTABA-S3150 motor is installed between every two modules. The robot measures 450 mm long and weighs 390 g in total.

A series of experiments are performed. The caterpillar robot successfully executes the proposed climbing gait on a stucco-like wall, with a slope angle of 72°. One moving cycle is shown in Fig. 18. The robot can perch on the wall firmly in our experiments, and the deformation of the compliant toes indicates the reduction in the sliding force.

The initial step length D_1 is about 5 mm, while the eventual step length D_2 can be only up to 3 mm due to the deviations from joint angles, which are caused by inaccurate control during the pulse transmission. The duration to deliver one pulse from the tail module to the top head is about 11 s.

Some pulses have revealed that it is not very easy for a few spines to detach from the stucco-like wall. In addition, the collision between the spines and the wall is obvious when we speed up the climbing. To solve these problems, it is necessary to adjust the spines' dimensions and allocate the module's compliance to fit various wall surfaces more suitable in next stage work.

https://doi.org/10.1017/S0263574714002446 Published online by Cambridge University Press

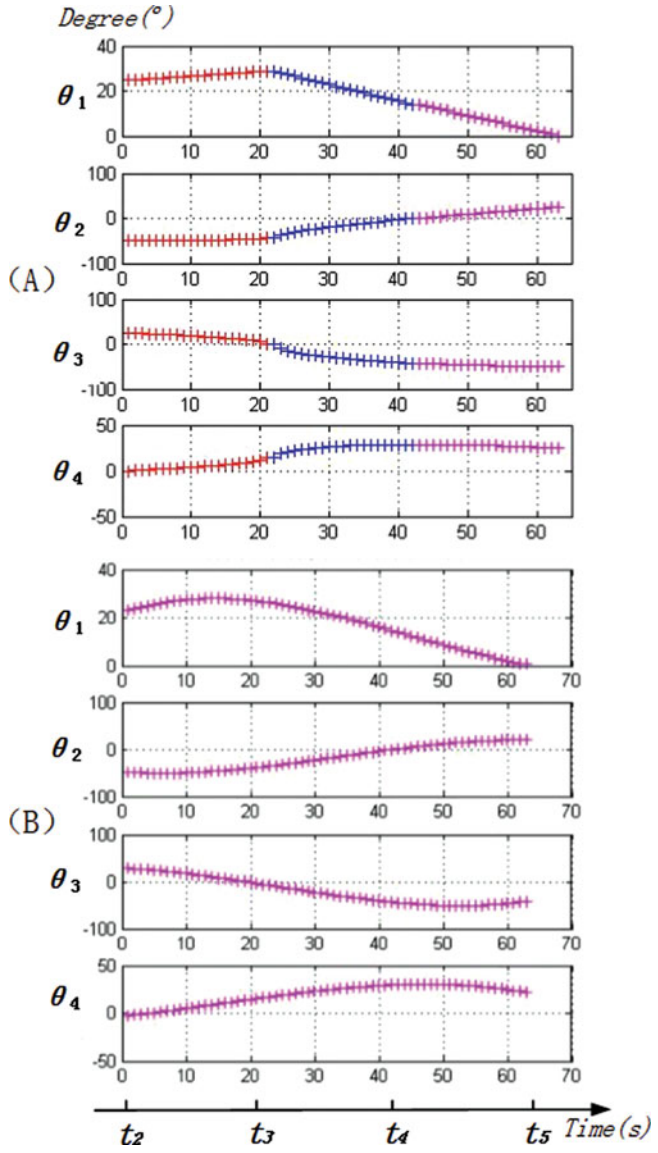

Fig. 15. The relevant joints' values during one pulse. Fig (A) is the solution of Eqs. (10)–(13) by MATLAB, which consists of process 1 (0 s–21 s), process 2 (21 s–42 s) and process 3 (42 s–63 s). Fig (B) is the three-order approximation to the original data. The smooth curve can be adopted in the controller program.

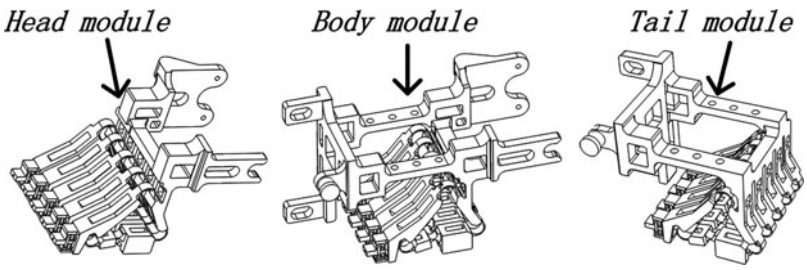

Fig. 16. Modules of the caterpillar robot.

https://doi.org/10.1017/S0263574714002446 Published online by Cambridge University Press

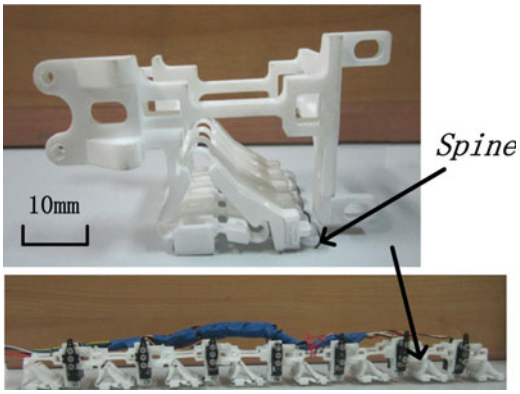

Fig. 17. The assembled caterpillar robot and one of its Nylon modules manufactured by 3D printer using Laser sintering rapid prototyping technology. Five micro spines are installed on each module in parallel.

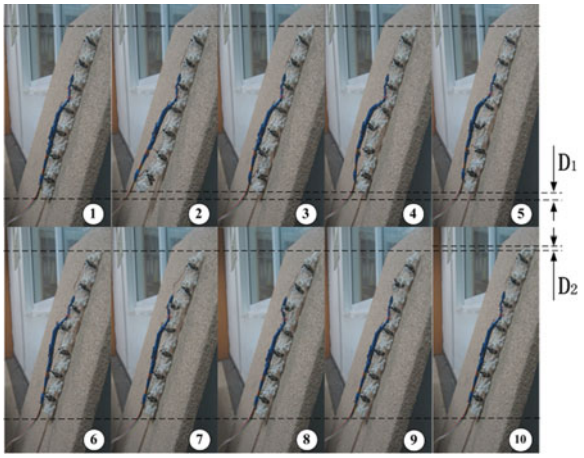

Fig. 18. Experiments of the prototype climbing on the stucco-like wall, showing the process of one moving cycle.

Although compliant modules are taken into account, the internal forces between the links cannot be completely eliminated because of the inaccurate open-loop control.

5. Conclusion

Based on the assumption of a spine's actual trajectory, a planar four-link compliant mechanism is brought up to drive the spines for reliable engagement. A step further, the model of one robot module is built, the parameters of the module are analyzed, and the driving torque of the active joint is calculated. By simulation, the spine trajectory and the compliant driving mechanism are testified. To build a caterpillar robot, the climbing gait is proposed, and the values of the moving joints angle is given by MATLAB for the sake of control program. Experiments on stucco-like wall are performed. The result proves the feasibility of the compliant module design. The future work will be focused on building a more precise model with the effect of damping in consideration. Besides, a close-loop control system will be developed to improve the climbing performance.

Acknowledgements

This paper is sponsored by the National Natural Science Foundation of China, No. 51075015.

References

1. Z. Yuanming, T. Dodd, K. Atallah and I. Lyne, "Design and Optimization of Magnetic Wheel for Wall and Ceiling Climbing Robot," *International Conference on Mechatronics and Automation*. (2010) pp. 1393–1398.
2. S. H. Kim, S. Hashi and K. Ishiyama, "Magnetic actuation based snake-like mechanism and locomotion driven by rotating magnetic field," *IEEE Trans. Robot.* **47**, 3244–3247 (2011).
3. Z. Houxiang, Z. Jianwei, L. Rong, W. Wei and Z. Guanghua, "Design of a Climbing Robot for Cleaning Spherical Surfaces," *IEEE International Conference on Robotics and Biomimetics (ROBIO)*. (2005) pp. 375–380.
4. H. Prahlad, R. Pelrine, S. Stanford, J. Marlow and R. Kornbluh, "Electroadhesive Robots-wall Climbing Robots Enabled by a Novel, Robust, and Electrically Controllable Adhesion Technology," *IEEE International Conference on Robotics and Automation*. (2008) pp. 3028–3033.
5. A. Yamamoto, T. Nakashima and T. Higuchi, "Wall Climbing Mechanisms Using Electrostatic Attraction Generated by Flexible Electrodes," *International Symposium on Micro-NanoMechatronics and Human Science*, (2007) pp. 389–394.
6. A. Sintov, T. Avramovich and A. Shapiro, "Design and motion planning of an autonomous climbing robot with claws," *Robot. Auton. Syst.* **59**, 1008–1019 (2011).
7. J. D. Dickson and J. E. Clark, "Design of a multimodal climbing and gliding robotic platform," *IEEE/ASME Trans. Mechatronics* **18**, 494–505 (2013).
8. Y. S. Li, A. Ahmed, D. Sameoto and C. Menon, "Abigaille II: toward the development of a spider-inspired climbing robot," *Robotica* **30**, 79–89 (2012).
9. D. Sameoto, Y. S. Li and C. Menon, "Multi-scale compliant foot designs and fabrication for use with a spider-inspired climbing robot," *J. Bionic Eng.* **5**, 189–196 (2008).
10. P. Boscariol, M. A. Henrey, Y. S. Li and C. Menon, "Optimal gait for bioinspired climbing robots using dry adhesion: a quasi-static investigation," *J. Bionic Eng.* **10**, 1–11 (2013).
11. A. T. Asbeck, S. Kim, M. R. Cutkosky, W. R. Provancher and M. Lanzetta, "Scaling hard vertical surfaces with compliant microspine arrays," *Int. J. Robot. Res.* **25**, 1165–1179 (2006).
12. K. Je-Sung and C. Kyu-Jin, "Omegabot: Crawling Robot Inspired by Ascotis Selenaria," *IEEE International Conference on Robotics and Automation (ICRA)*. Anchorage, AK, (2010) pp. 109–114.
13. A. L. Desbiens, A. Asbeck and M. Cutkosky, "Hybrid Aerial and Scansorial Robotics," *IEEE International Conference on Robotics and Automation (ICRA)*. Anchorage, AK, (2010) pp. 72–77.
14. L. Tin Lun and X. Yangsheng, "Climbing strategy for a flexible tree climbing robot-treebot," *IEEE Trans. Robot.* **27**, 1107–1117 (2011).
15. A. Parness, M. Frost, J. A. King, N. Thatte, K. Witkoe, M. Nevarez *et al.*, "Video Presentation of A Rock Climbing Robot," *IEEE/RSJ International Conference on Intelligent Robots and Systems (IROS)*. (2013) pp. 2076–2076.
16. W. Wang and L.-c. Zhao, "A Method to Reduce the Sliding Force on Adhering Points of Caterpillar Climbing Robot," *International Conference on Information and Automation (ICIA)*. Shenyang, China, (2012) pp. 715–720.
17. W. R. Provancher, J. E. Clark, B. Geisler and M. R. Cutkosky, "Towards Penetration-Based Clawed Climbing," *7th International Conference on Climbing and Walking Robots (CLAWAR 2004)* Madrid, Spain, (2004) pp. 961–970.
18. W. Wang, K. Wang and H. X. Zhang, "Crawling gait realization of the mini-modular climbing caterpillar robot," *Prog. Natural Sci.* **19**, 1821–1829 (2009).
19. W. Wang, H. X. Zhang, K. Wang, J. W. Zhang and W. H. Chen, "Gait control of modular climbing caterpillar robot," *IEEE/ASME International Conference on Advanced Intelligent Mechatronics*, (2009) pp. 957–962.

https://doi.org/10.1017/S0263574714002446 Published online by Cambridge University Press